Engineering Structures 243 (2021) 112529

Contents lists available at ScienceDirect

Engineering Structures

journal homepage: www.elsevier.com/locate/engstruct

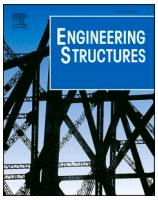

Quantification of damage evolution in masonry walls subjected to induced seismicity

Vasilis Sarhosis [a], Dimitris Dais [a,b], Eleni Smyrou [b,*], İhsan Engin Bal [b], Anastasios Drougkas [a]

[a] School of Civil Engineering, University of Leeds, LS2 9JT Leeds, UK
[b] Research Center for Built Environment NoorderRuimte, Hanze University of Applied Sciences, Zernikeplein 11, Groningen, the Netherlands

ARTICLE INFO

Keywords:
Masonry
Distinct element method
Cumulative damage
Induced vibrations
Crack-based damage quantification

ABSTRACT

This paper aims to quantify the evolution of damage in masonry walls under induced seismicity. A damage index equation, which is a function of the evolution of shear slippage and opening of the mortar joints, as well as of the drift ratio of masonry walls, was proposed herein. Initially, a dataset of experimental tests from in-plane quasi-static and cyclic tests on masonry walls was considered. The experimentally obtained crack patterns were investigated and their correlation with damage propagation was studied. Using a software based on the Distinct Element Method, a numerical model was developed and validated against full-scale experimental tests obtained from the literature. Wall panels representing common typologies of house façades of unreinforced masonry buildings in Northern Europe i.e. near the Groningen gas field in the Netherlands, were numerically investigated. The accumulated damage within the seismic response of the masonry walls was investigated by means of representative harmonic load excitations and an incremental dynamic analysis based on induced seismicity records from Groningen region. The ability of this index to capture different damage situations is demonstrated. The proposed methodology could also be applied to quantify damage and accumulation in masonry during strong earthquakes and aftershocks too.

1. Introduction

Ensuring the security of energy supply and providing competitive energy costs are vital and of strategic importance for Europe. In the last decade, with the pressure to increase local energy supply by unlocking the energy potential of the ground, induced seismicity in the northern part of Europe has considerably increased [1]. At the same time, the existing building stock in the region has not been designed to sustain such seismic demands. Consequently, structural and non-structural damages in buildings have been observed. For example, in Switzerland magnitudes of up to 3.5 Richter have been reported, due to enhanced geothermal systems, resulting in cracks on walls alongside non-structural damages [2]. The resulted damage claims are in excess of 7–20 million Swiss Francs. Similar situation is also described in Groningen, the Netherlands. In this case, the seismicity is related to the hydraulic fracturing process for the extraction of natural gas from deep geological formations. Back in 1991, the first induced seismicity was recorded in the gas field. The local magnitude (ML) was 2.4. In the subsequent years, more than 1,300 small in magnitude earthquakes were reported in the region, the largest of which was the one in 2012 with local magnitude equal (ML) to 3.6 [3]. Along the period of seismic shakings in the Groningen, the damage claims from citizens increased. For example, for the period 2012 to 2016, an average of € 374 million per year was spent on compensation for damages as consequence of gas extraction, which accounts for approximately 3% of the average revenues from gas extraction during the same period [4]. On top of this, issues related to devaluation of the real estate market and buyout of properties, expenses for the seismic retrofit of the structures and cost of lawsuits need to be accounted for [5].

Most of the building stock in the Northern part of Europe consists of low-rise unreinforced masonry (URM) constructions [6]. Typical architectural features (e.g., large openings for windows and doors, use of single leaf walls in domestic houses etc.) in unreinforced masonry structures and the lack of seismic design provisions during their construction signify that the building stock is seismically vulnerable even under low in magnitude seismic events. Recently, several experimental and analytical studies have been carried out to assess the mechanical behaviour and evaluate the damage of typical unreinforced masonry constructions subjected to recursive, frequent but low-amplitude seismic loads. For example, [7–9] demonstrated that masonry structures are

* Corresponding author.
E-mail address: e.smyrou@pl.hanze.nl (E. Smyrou).

https://doi.org/10.1016/j.engstruct.2021.112529
Received 14 February 2021; Received in revised form 19 April 2021; Accepted 9 May 2021
Available online 21 June 2021

vulnerable to recursive load and damage can be captured by the drift ratio as well as the length of cracks extent in the structure during shaking. The same year, Godio et al. [7], undertook a series of experimental tests on URM wall panels to compare the drift ratios of walls under cyclic and monotonic loads. From the analysis of the results, it was shown that the ultimate drift of walls subjected to cyclic loading is approximately half of that when subjected to monotonic loading. Graziotti et al. [10] undertook an experimental campaign involving shaking table tests on a full scale two-storey URM building. The building was constructed to represent the end-unit of a terraced house with architectural features like the ones found in Netherlands e.g., large openings and cavity wall composed of an inner load bearing leaf and an outer leaf having aesthetic and weather protection functions. The input motions were representative of the induced seismicity ground motions found in the Groningen region and two damage limits identified. The first damage limit considered was related to "no damage" and was set to 0.07% of the maximum interstorey drift at the first floor. The second damage limit related to "minor structural damage" and was set to 0.12% of the maximum interstorey drift at first floor level. An important finding from this work is that although the residual drift of the wall was zero, cracks in the unreinforced masonry opened and closed until they become evident when the second damage limit was reached. Therefore, quantifying damage only on the residual drift is considered to be a conservative approach. Therefore, more robust approaches need to defined and these should account for the initiation and propagation of damage as the seismic excitations take place in a structure [11,43,44].

In general, induced seismicity is described by high recurrence of seismic events. So, structural health monitoring (SHM) may be employed for damage detection at a structural level [12–15,42]. A tool for non-destructive method for damage identification and quantification is digital image correlation (DIC). DIC is an optical method that employs tracking and image registration techniques for accurate full filed measurements of displacements and strains [16–18]. DIC along with acoustic emission were utilized in the past to detect, monitor and quantify damage propagation [19,20]. In particular, different studies utilized DIC techniques for the quantification of the development of damage caused by small to moderate seismicity. Abbiati et al. [2] undertook an experimental campaign attempting to produce a probabilistic model for quantifying plaster cracks on URM structures due to induced seismicity. In order to quantify the initiation and accumulation of damage, a "damage score" was proposed based on Von Mises strain field estimations [2]. More recently, Korswagen et al. [9] carried out an experimental campaign to quantify light damage on URM structures due to repeated horizontal loads. DIC was utilized to precisely capture the initiation and propagation of cracks during the experiments. A dimensionless damage parameter was introduced based on the number of cracks, their width and length [9]. Overall, DIC is a powerful tool in the unambiguous detection of damage in masonry. However, it could be disadvantageous in distinguishing between shear and tensile cracks, both of which develop in masonry under seismic loading. Coupling with numerical analysis, this ambiguity can be eliminated, and the quantification of shear and tensile damage can be properly achieved.

The length, width, pattern and distribution of cracks in the structure, are important indicators to characterise structural damage in masonry [15,21–23]. In order to provide a quantitative assessment of shear-cracked reinforced concrete (RC) structures, a crack-based analysis procedure has been presented by Zaborac at al. (2020) [24]. The suggested methodology utilized a combination of measured and estimated concrete cracking data (e.g. crack widths, spacing of cracks, inclination of cracks etc.) as primary input to predict the residual shear capacity of a RC beam [24]. Acceptance limits of the structural response of RC walls were suggested based on inter-story drift ratios, residual crack width and total damaged area (i.e. the area of cracks) [25]. Regression models, capable of estimating the maximum lateral drift experienced by a damaged RC column based solely on quantitative data extracted from images of any cracks were developed [26]. A computer vision approach was followed to generate a quantitative assessment of damage and load levels based on surface crack patterns for RC structural elements [27]. The results obtained were set as a baseline for the potential of the proposed method and its limitations [27].

Based on the literature review, it is noted that studies on URM are rather limited even though crack-based assessment has attracted the interest of the research community. The aim of this study is to investigate the quantification of damage on URM structures which takes into consideration the initiation and propagation of damage due to earthquake excitations. A dataset from experimental test results of cantilever masonry walls subjected to in-plane quasi-static cyclic was considered. The experimentally obtained crack patterns were investigated and their correlation with damage propagation was studied. Using software based on the Distinct Element Method (DEM), a numerical model was developed and validated against a series of full-scale experimental tests obtained from the literature. Wall panels representing common typologies of house façades of URM buildings in Northern Europe, i.e., near the Groningen gas field, were numerically investigated. The accumulated damage within the seismic response of the masonry walls was investigated by means of representative harmonic load excitations and an incremental dynamic analysis based on induced seismicity records from the Groningen region. A damage index based on cracking distribution and drift ratio is proposed and applied to the numerical findings while common trends between the numerical and experimental data were highlighted. The damage indexing differentiates between shear and tensile cracks, which can be accomplished unambiguously only through numerical analysis. Therefore, the indexing method is envisaged as mainly applicable for the quantification of damage at structural level obtained from numerical analysis as a complement to optical monitoring and visual inspection.

2. Damage index equation

Existing masonry structures, especially historical ones, are usually characterized by their low bond strength. Low bond strength masonry refers to masonry in which the tensile and shear bond at the unit-mortar interface is so low that it has a dominant effect on the mechanical behaviour of masonry, including the formation of cracks and the formation of the collapse mechanisms [28]. Therefore, any damage indexing scheme for masonry should consider the proportion of joints that have undergone inelastic slip or tensile/shear opening (i.e., cracking) of the mortar joints. Also, when a structure is subjected to lateral loads, it sustains lateral deflections. At structural element level, drift can be estimated as the difference in lateral deformation between two stories of a structure due to the application of later loads (such as seismic loads). In its simple format, for a single-story building, lateral drift equals the amount of horizontal displacement at the top. Lateral drift is an important indicator of the level of damage in a building after an earthquake [29]. Also, based on the inter-story drift (ISD) ratio, the building can be classified as serviceable, safe, or unsafe. Typically, the ISD ratio should not pass a certain drift limit to keep it at a certain performance level (ASCE 2000). The ASCE 7–16 [30] standard common usage for building design of allowable drift limit is in the order of 1/600 to 1/400 of the building or story height. Also, for buildings, EN 1998–1 [31] establishes the following limits to the inter-storey drift (relative displacement divided by the inter-storey height) due to the frequent earthquake (this refers to serviceability seismic action):

- 0.5% for buildings having non-structural elements of brittle materials attached to the structure.
- 0.75% for buildings having ductile non-structural elements.
- 1.0% for buildings having non-structural elements fixed in a way so as not to interfere with structural deformations or without non-structural elements.

Consequently, a damage index (*DI*) equation is proposed here in

which can be used to quantify damage evolution on URM structures subjected to seismic excitations. The *DI* equation consists of three damage parameters which include: a) the extent of drift ratio (DI_{drift}); b) the length of joints opened (DI_{open}); and c) the length of joints at shear failure (or slippage) (DI_{slip}):

$$DI = 1 - \left(1 - DI_{\text{drift}}\right) \times \left(1 - DI_{\text{open}}\right) \times \left(1 - DI_{\text{slip}}\right) \quad (1)$$

$$DI_{\text{drift}} = \frac{\delta}{\delta_{\text{limit}}} \quad (2)$$

$$DI_{\text{open}} = \frac{\text{Length of joints opened}}{\text{Total length of joints}} \quad (3)$$

$$DI_{\text{slip}} = \frac{\text{Length of joints slipped}}{\text{Total length of joints}} \quad (4)$$

where, DI_{drift} is the drift ratio (δ) by a drift limit value (δ_{limit}) which refers to the near collapse state of the structure under investigation. In this study, the drift limit value was taken as 2% (as per Eurocode 8 [31] or NTC 2008 [32]). DI_{open} and DI_{slip} relate to the length of joints that opened due to tension and the length of joints slipped (or at shear limit) due to shear respectively, divided by the total length of joints. In this way, the DI_{open} and DI_{slip} are normalized metrics of the cracks along the surface of the wall and are independent of the dimensions of the structural element. According to Burland [33], cracks greater than 0.1 mm in width are visible to the naked eye. This value of inelastic relative displacement at the joint was adopted as the criterion for registering a joint as 'opened'. The value of the calculated *DI*and the individual components DI_{drift}, DI_{open}, and DI_{slip} ranges from 0 (no damage) to 1 (catastrophic collapse or all joint failed or drift limit reached).

3. Overview of discrete element method for modelling masonry walls

The proposed damage indexing scheme was integrated to a modelling approach based on the discrete element method to study the mechanical behaviour of masonry structures under seismic loading. The discrete element method (DEM) belongs to the dicontinuum analysis approaches. The Universal Distinct Element Code (UDEC) is a two-dimensional command driven software that was developed by Cundall [34] in early 1970s for solving problems related to sliding of rock masses and falls within the DEM. Since then, the code has been used with success to simulate the static and dynamic behaviour of blocky systems including masonry structures e.g. [36,37]. The code's framework is different to that of the well-known finite element method (FEM). Within UDEC, a masonry wall can be considered as a series of distinct blocks separated by zero thickness interfaces. Such zero-thickness interfaces can open and close depending on the stresses they sustain [41]. Masonry units are represented by blocks which could have any geometric shape and can be assigned different mechanical properties even in the same model. The DEM can be used to realistically represent geometrical, physical, and mechanical characteristics of a masonry structure as opposed to the numerical methods in which continuity theories exists and masonry is considered as a simplification into an unrealistic continuum [41]. Another characteristic of the DEM is that large displacements and rotations of the masonry units are allowed and that detection of contacts between neighbouring masonry units and updating of contacts is occurring simultaneously and as the simulation proceeds [35]. In addition, the DEM can make use of an explicit dynamic solution algorithm scheme which allows real dynamic analysis to be undertaken.

3.1. Representation of the masonry units in a masonry wall

When defining the model in UDEC, a single block covering the domain to be analysed is considered. The geometric features of the model are then introduced by discretizing the block into smaller ones (e.g., masonry units) whose boundaries represent discontinuities (e.g., mortar joints). It is these discontinuities which allow the interaction between blocks to take place as the simulation proceeds. Since the mortar joints are simulated by a zero-thickness interface, the size of the masonry units has to be to be expanded slighted (e.g. half of the mortar thickness in each direction) to accommodate this. In general, blocks can take any geometry and could differ from each other in size and shape. Individual blocks can be rigid or deformable. Rigid blocks can be used when the behaviour of the system is dominated by the joints (i.e., in cases where masonry units are strong, the mortar joints are weak, and failure is a result of debonding of masonry units to mortar joints or failure of the mortar joints). Deformable blocks are used when deformation of masonry units plays a role in the mechanical response of the system or when internal stresses in masonry units needs to be estimated. The complexity of the deformation of the blocks depends on the number of zone elements into which they are divided (i.e., finite discretization), and the constitutive law assigned to them. The constitutive model assigned to the zones could be either linear elastic or non-linear elastic and the strain for each separate block can be estimated. The material parameters for the linear elastic model are the unit weight of the brick, the compression modulus (K) and the shear modulus (G).

$$K = \frac{E}{3(1-2v)} \quad (5)$$

$$G = \frac{E}{2(1+v)}, \quad (6)$$

where E is the Young modulus and v is the Poisson's ratio of the brick. Also, the size of simulation is limited by the number of masonry units which is a function of the available computational power (see Fig. 1).

3.2. Representation of mortar joints in a masonry wall

Within the discrete element method, mortar joints are represented by zero-thickness interfaces. At each interface, masonry units are connected cinematically to each other by contacts; the so called contact hypothesis approach [38]. These contact points are positioned at the outside perimeter of the masonry units. For deformable blocks, the contact points are located at the edges or corners of the blocks and the zones. In this way, geometric interaction between the blocks is allowed. A significant advantage of the contact hypothesis method is its ability to mesh the block independently without the need to match nodal points. So, the more the number of contact points, the higher the accuracy of the stress distribution in the blocks. The contact points in UDEC are "soft". This means that the contact forces are generated as a result of interpretation of adjacent blocks. The amount of interpenetration is controlled by the user and does influence the computational time. At each contact point there are two spring connections (Fig. 2). The springs allow the transfer of a normal force or a shear force from one block to the other. In the normal direction, the mechanical behaviour of mortar joints can be represented using the following equation:

$$\Delta\sigma_n = -k_n \cdot \Delta u_n \quad (7)$$

where k_n is the normal stiffness of the contact (stress deformation characteristic), $\Delta\sigma_n$ is the change in normal stress and Δu_n is the change in normal displacement. Similarly, in the shear direction the mechanical behaviour of the joints is controlled by constant shear stiffness k_s using the following expression:

$$\Delta\tau_s = -k_s \cdot \Delta u_s \quad (8)$$

where $\Delta\tau_s$ is the change in shear stress and Δu_s is the change in shear displacement along the joint. Stresses calculated at grid points along contacts are submitted to the Mohr-Coulomb failure criterion which limits shear stresses along joints. The following parameters are used to

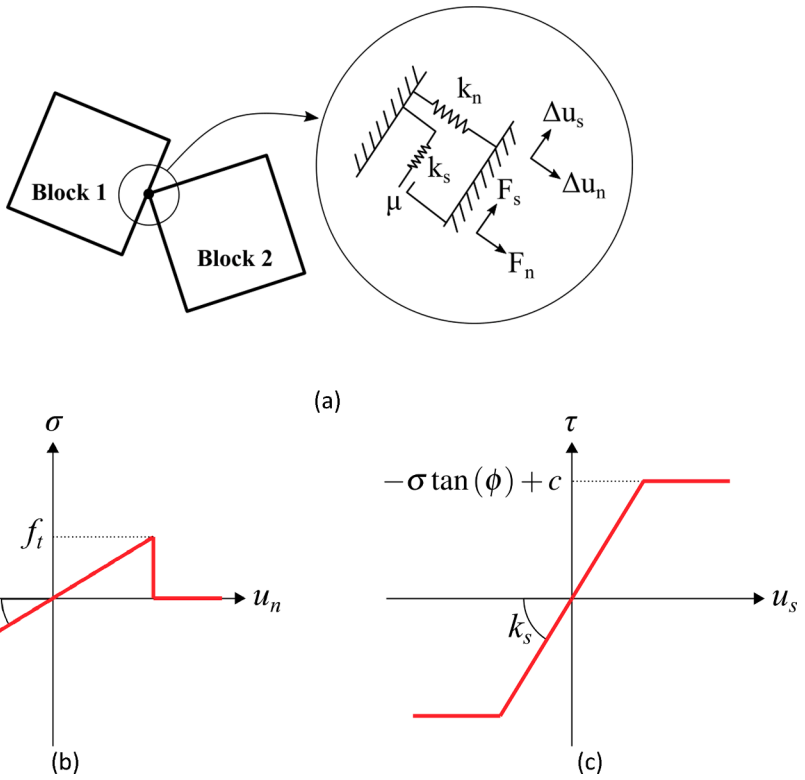

Fig. 1. Mechanical representation: (a) contact between blocks; joint behaviour under (b) normal and (c) shear loads.

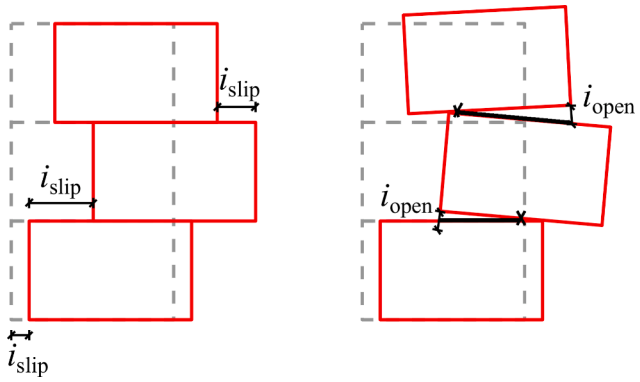

Fig. 2. Representation of joints opening and joint at shear limit. Parameters i_{slip} (length of joint slipped) and i_{open} (length of joint opened) recorded during the simulation.

define the mechanical behaviour of the contacts: the normal stiffness (k_n), the shear stiffness (k_s), the friction angle (φ), the cohesion (c), the tensile strength (f_t) and the dilation angle (ψ).

A problem often encountered when modelling masonry is the unrealistic response when brick interaction occurs close to or at two opposing brick contacts. At this point, numerically, blocks may be locked or hung-up due to the modelling assumptions that brick corners are sharp or have infinite strength. In a real masonry structure this will only occur because of stress concentrations. Simulating such a phenomenon is impractical. A realistic representation can be achieved by rounding the corners of the blocks so that they can smoothly slide past one another when two opposing corners interact. A short corner rounding length (e.g. 1% of the block's length) gives a good level of accuracy.

3.3. Numerical solution

Estimation of motion in masonry units is made using the force displacement law at all contacts and the Newton's Second Law of motion at each time increment using the central difference method. Contact forces can be obtained from the force–displacement law. Similarly, the motion of the masonry units can be obtained from the known forces acting on the nodes using the Newton second law. For the numerical solution, a dynamic relaxation procedure is adopted. Adaptive damping is used for convergence to static solution. A limit step can be defined by the user which helps to avoid numerical instabilities. The time-step can be calculated using the equation below:

$$\Delta t_n = 2f\sqrt{\frac{M_n}{K_n}} \tag{9}$$

where and K_n is the overall stiffness of the units and contacts connected to the node, M_n is the nodal mass, and f is a user-defined factor which controls the time-step [35]. The length of the computational effort can be minimized by parallel processing, scaling up the number of units and scaling up the length of simulation.

A characteristic feature of UDEC is the geometric non-linearity of the intact bricks to be modelled. In other worlds, the displacement of the bricks due to shear and opening up of the interface can be immediately included in the calculations. So, it is possible that bricks which were originally adjacent to each other could either become partially or entirely loosened from each other, or new contact points could be formed between bricks that were initially not next to each other. This is significant feature of UDEC when modelling problems involving discontinuities such as low bond strength masonry, where the predominant failure mechanism is due to the de-bonding of the bricks or blocks from the mortar, as the location and the magnitude of surface crack widths within a masonry structure can be determined realistically. Detecting and updating brick contacts in a numerical model is the most time-consuming part of the software's calculation.

3.4. Implementation of damage indexing equation in DEM

Mortar joints can open, close and slip depending on the stresses acting on them (Fig. 2). Criteria for joint opening and slip are based on the magnitude of normal displacement or on the shear stresses levels. Joint opening occurs when the normal stress σ_n at a contact exceeds the tensile strength f_t, a condition expressed by the equation:

$$\sigma_n \geq f_t \tag{10}$$

The value of f_t is defined by the user and can be taken experimentally by undertaking small scale testing e.g. crossed brick couplets. Upon reaching this condition, the normal stress is reduced to zero and the tensile strength of the interface vanishes. According to the relative displacement threshold of 0.1 mm established, joints are marked as opened when this threshold is exceeded. However, this threshold value can be assigned by the user.

Slippage between the units will occur when the shear force at a contact reaches a critical value τ_{max} defined by the Mohr Coulomb criterion:

$$\tau_s \geq c + \sigma_n \tan(\varphi) = \tau_{max} \tag{11}$$

where τ_s is the shear stress at the joint, c is the cohesion and φ is the friction angle. The value of cohesion and friction can be obtained from small scale tests such as triplet shear tests.

3.5. Validation of DEM for masonry walls

A two-dimensional numerical model based on DEM was developed to estimate and understand the extent of damage accumulation in masonry walls with and without openings subjected to induced seismicity events. All walls had dimensions equal to 4 m width and 2.75 m height (Fig. 3), typical in Dutch construction practice. One solid (Fig. 3a) and two perforated walls, either symmetric (Fig. 3b) or asymmetric (Fig. 3c), were examined. The size of the opening was set to 2 m by 2.5 m. Such large openings on the façade are quite common in the building inventory within the Groningen gas field. The vertical sides of the wall were left free. In addition, the top of the wall was also free to rotate creating a cantilever condition. A vertical pre-compression equal to 0.3 N/mm^2 was applied at the top of the wall during loading. Each brick of the masonry wall panel was represented by a deformable block separated by zero thickness interfaces at each mortar bed and perpendicular joint. To allow for the 10 mm thick mortar joints in the real wall panels, each deformable block was based on the nominal brick size increased by 5 mm in each face direction resulting in a model block size of 225 mm × 102.5 mm × 75 mm.

The mortar joints were represented by zero-thickness interfaces between the masonry units. In this study, mortar joints were assumed to behave in an elastic-perfectly plastic Coulomb slip-joint area contact option. This provides a linear representation of the mortar joint stiffness and a yield limit based upon elastic normal (k_n) and shear (k_s) stiffness, frictional (φ), cohesive (c) and tensile (f_t) strength characteristics of the mortar joints. In addition, if the bond tensile strength or shear strength is exceeded in the numerical calculation, then the tensile strength and cohesion are reduced to zero. Also, the dilation angle was assumed zero, as per [36].

The developed model was validated against experimental results obtained from Graziotti et al. [10]. The material properties of the zero-thickness interfaces and the masonry units are presented in Table 1 and Table 2 respectively. For further information regarding the development of the computational model, the reader is referred to [11].

A comparison between the experimentally obtained behaviour and the numerical model is illustrated in Fig. 4 in terms of initial stiffness and hysteretic behaviour. Overall, good agreement was obtained, with the stiffness and peak force being approximated with very good accuracy and the unloading/reloading stiffness being reasonably well reproduced.

A comparison of the experimental against the numerically predicted crack patterns is shown in Fig. 5. Considering the inherent variability of masonry, the numerical model was able to capture the failure mode fairly accurately.

4. Application of damage indexing in walls under harmonic loading

Using the *DI* equation (eq. (1)), estimates of the evolution of damage in masonry wall panels subjected to harmonic loading of different amplitudes and periods were estimated. The solid wall has a natural period of 0.06 s, while the period of the perforated wall panels is approximately 0.2 s. The models were subjected to sinusoidal acceleration loading with varying amplitude (0.01 g, 0.025 g, 0.05 g, 0.075 g and 0.1 g) and

Table 1
Material properties of the zero-thickness interfaces used in the numerical model.

Joint normal stiffness	Joint shear stiffness	Joint friction angle	Joint tensile strength	Joint cohesive strength
k_n(N/m^3)	k_s(N/m^3)	φ(deg)	f_t(N/m^2)	c(N/m^2)
12×10^{11}	4×10^{11}	32	0.21×10^6	0.24×10^6

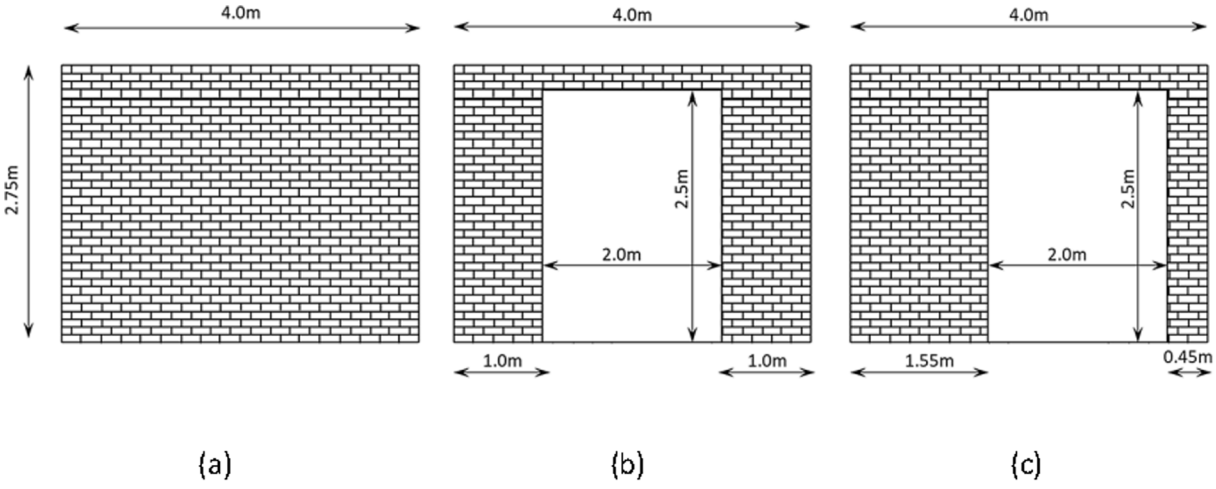

Fig. 3. The geometry of the models developed: (a) wall panel with no opening/solid wall; (b) wall panel with symmetric opening; (c) wall panel with asymmetric opening.

Table 2
Material properties of the masonry units used in the numerical model.

Elastic modulus of brick E(N/m^2)	Bulk Modulus K(N/m^2)	Shear Modulus G(N/m^2)
5.20×10^9	2.90×10^9	2.16×10^9

excitation periods (0.06 s, 0.2 s, 0.33 s and 1 s). The acceleration amplitude was up to 0.1 g. This is an acceptable level of acceleration considering that the highest peak ground acceleration (PGA) ever recorded in the Groningen gas field was 0.11 g in the 2018 Zeerijp earthquake (Fig. 10). The applied harmonic loadings are presented in Fig. 6. From the results of the analyses, it was concluded that, there was slight damage in the solid wall when subjected to low amplitude harmonic loadings and thus, for the shake of brevity, only the results from

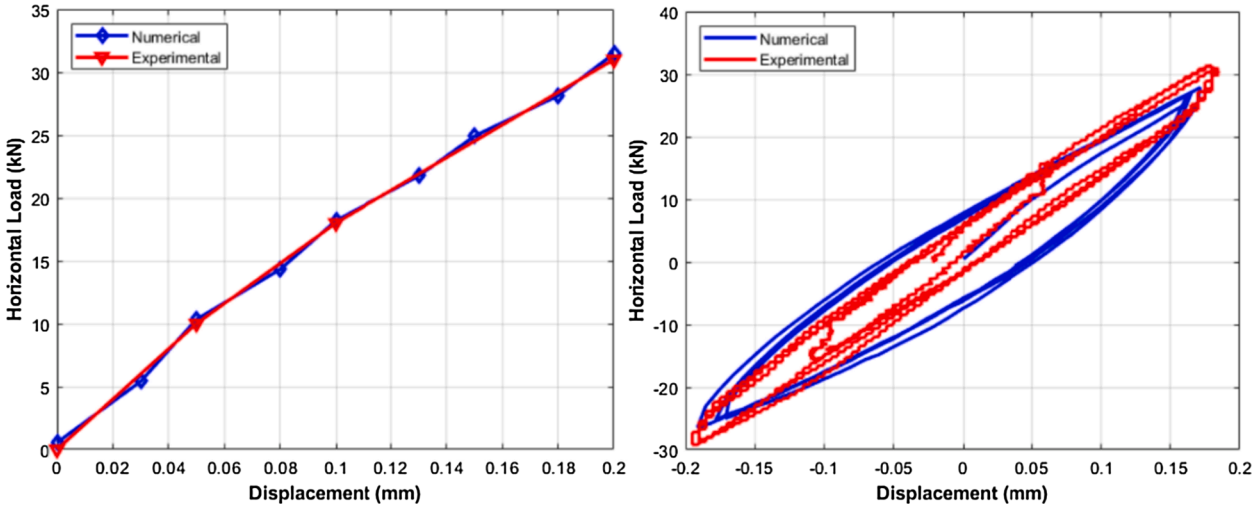

Fig. 4. Comparison of experimental against numerical results in terms of the initial stiffness for the squat model (left) and the first loading cycles (right).

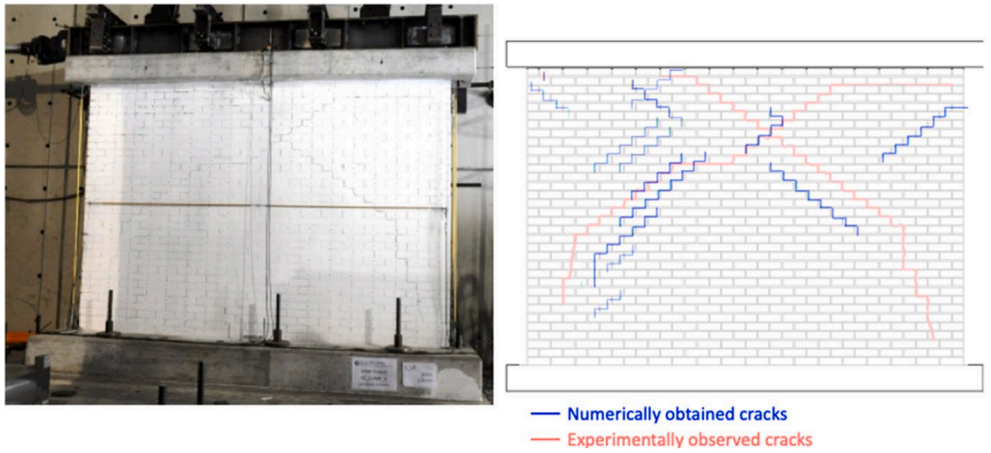

Fig. 5. Comparison of experimental (left) against numerical (right) failure mode.

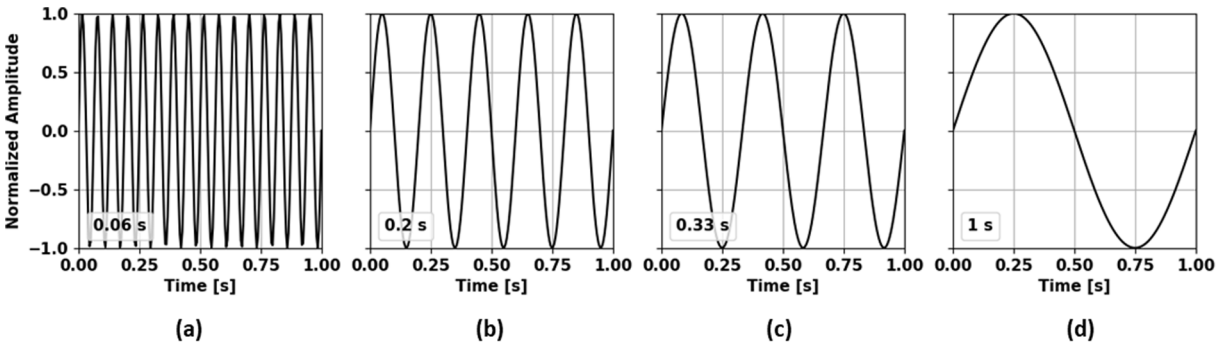

Fig. 6. The harmonic loadings applied in the numerical analyses with excitation period (a) 0.06, (b) 0.2, (c) 0.33 and (d) 1 s.

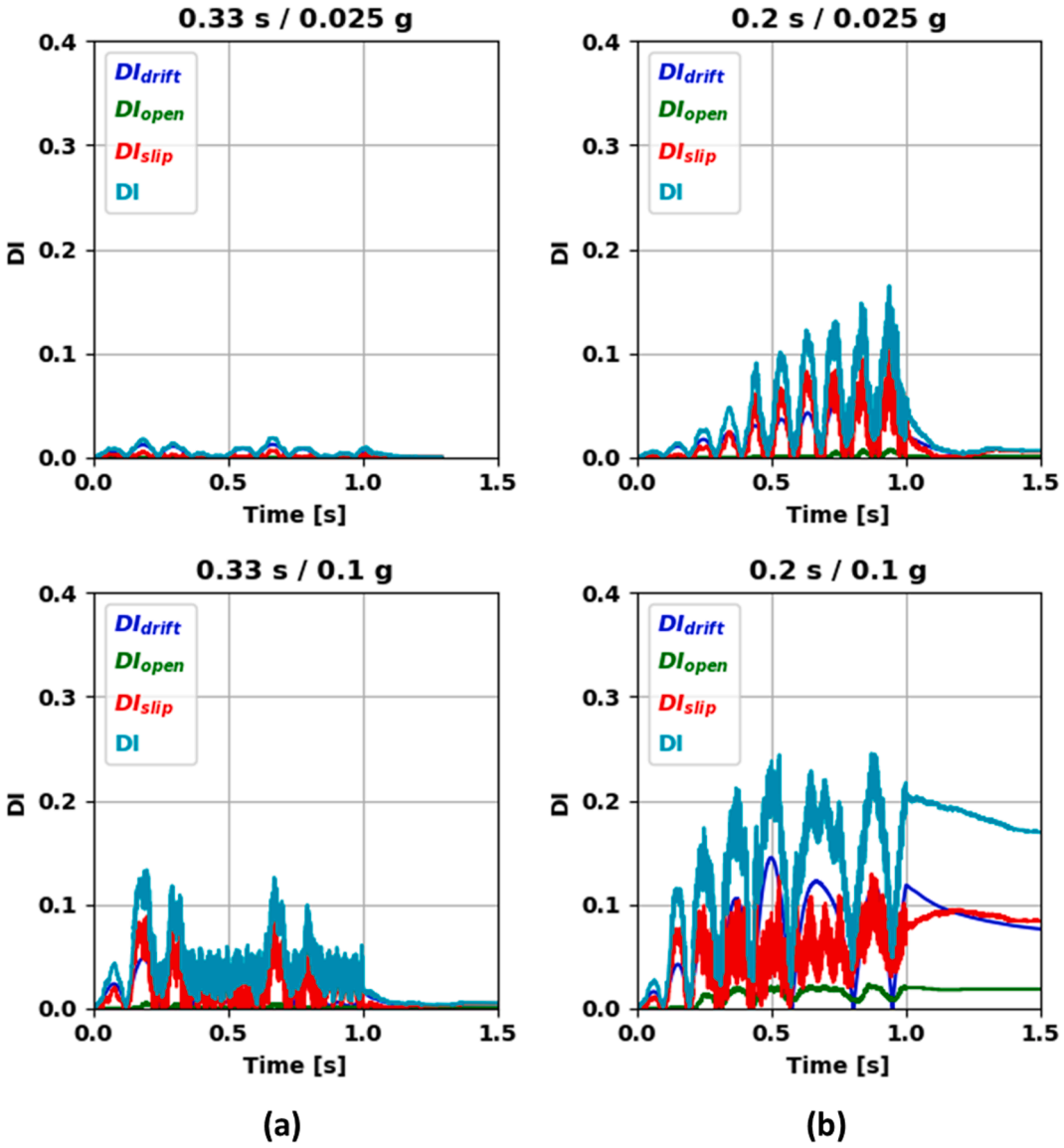

Fig. 7. The evolution of the damage indices DI_{drift}, DI_{open}, DI_{slip} and DI for the symmetric model for acceleration amplitudes 0.025 and 0.1 g and periods of excitation (a) 0.33 and (b) 0.2 s.

the perforated wall panels will be presented herein.

Fig. 7 shows the evolution of DI and its components (DI_{drift}, DI_{slip} and DI_{open}) over time for the URM wall with a symmetric opening when subjected to acceleration amplitudes equal to 0.025 and 0.1 g and excitation periods 0.33 s and 0.2 s. These accelerations correspond to low and moderate acceleration amplitude, respectively. The period of 0.2 s matches the natural frequency of the perforated walls, while the period 0.33 s is slightly higher of that of the natural frequency and thus resonance is not expected to occur in this case. When the wall was excited to a period of 0.33 s and acceleration amplitude equal to 0.025 g, the inflicted damage was negligible (Fig. 7a). When dynamic motion with period 0.33 s and acceleration 0.1 g was applied, the maximum value of DI was attained during the first cycle of the excitation and in the upcoming cycles the same value of DI was reached but this was not exceeded (Fig. 7a). For the wall subjected to a period of 0.2 s, the achieved maximum DI increased for every cycle of the harmonic signal for both acceleration amplitudes (see Fig. 7b). Similar response was obtained for the wall with asymmetric opening. Consequently, even slight difference between the frequency of the signal and the natural frequency of the modelled wall significantly altered the response of the structure. When resonance occurred, even for low acceleration, damage propagated further during the successive cycles, while when there was no period matching only for higher acceleration some extent of damage was recorded and did not spread additionally along consecutive load cycles.

Fig. 8 shows the maximum and residual values of the damage indices DI_{drift}, DI_{open}, DI_{slip} and DI for the wall with symmetric opening for the excitation periods considered. The asymmetric wall presents similar behaviour as the symmetric one and thus it was not deemed essential to be included here. When the wall was excited to a period of 0.06 s only slightly damage was recorded; even for higher amplitudes of acceleration. For the cases of period 0.33 s and 1 s, the maximum DI reported increased linearly as stronger motions were applied while residual damage was negligible. Since period 0.33 s falls closer to the natural period of the wall, higher damage was observed in terms of DI for the corresponding excitations. In particular for period 0.33 s and 1 s the maximum attained DI was 0.13 and 0.1 respectively.

When resonance took place, i.e. excitation period equal to 0.2 s, substantially higher damage was reached. Interestingly, for the higher acceleration values, i.e. 0.05, 0.075 and 0.1 g, the same values maximum DI_{open}, DI_{slip} were reached. This behaviour implied that the failure mechanism was fully activated, and any further damage was

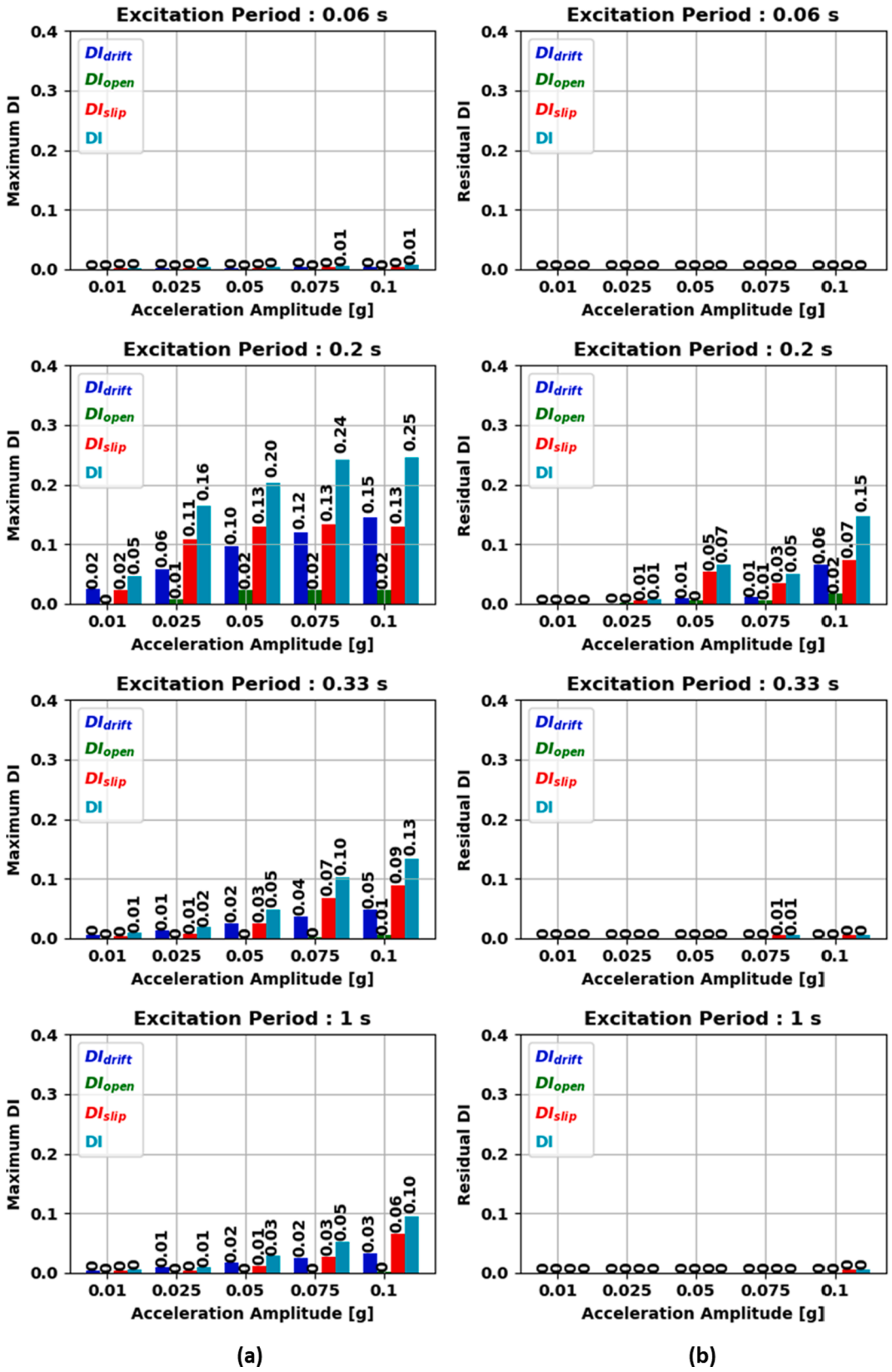

Fig. 8. (a) Maximum and (b) residual values of the damage indices DI_{drift}, DI_{open}, DI_{slip} and DI presented for the wall with symmetric opening. From top to bottom the graphs correspond to excitation period 0.06 s, 0.2 s, 0.33 s and 1 s respectively.

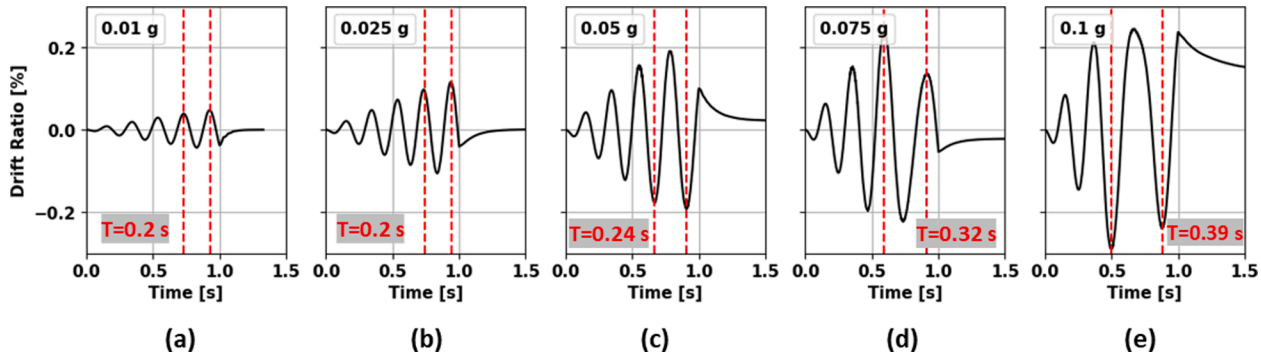

Fig. 9. The drift ratio time-history as obtained from the analyses with the wall with symmetric opening for excitation period 0.2 s is presented for acceleration amplitudes (a) 0.01 g, (b) 0.025 g, (c) 0.05 g, (d) 0.075 g and (e) 0.1 g. For each subplot, with red dashed lines is denoted the last full cycle as observed in the drift ratio time-history and its duration T is displayed as well. (For interpretation of the references to colour in this figure legend, the reader is referred to the web version of this article.)

expressed as further opening or sliding of the already formed cracks. On the other hand, the measured DI_{drift} steadily increased for higher accelerations. When the excitation period was 0.2 s, it was the only case where non-negligible residual damage was recorded. For the cases of the acceleration equal to 0.05 and 0.075 g, the residual damage was mostly expressed through cracks (opening or sliding). For the highest acceleration considered, that is 0.1 g, residual drift was noticed.

In Fig. 9, the drift ratio as obtained from the analyses with the wall with symmetric opening for excitation period 0.2 s is presented. One should mention that this excitation period matches the natural period of the walls with opening. The last full cycle is shown with red dashed lines and its duration T is displayed too (Fig. 9). From Fig. 9, it is noticed that the duration of the last full cycle increased when higher acceleration amplitudes were applied. For accelerations 0.01 g and 0.025 g, the duration T equalled 0.2 s. On the other hand, this duration reached 0.24 s, 0.32 s and 0.39 s for accelerations 0.05 g, 0.075 g and 0.1 g respectively (Fig. 9). This response is related to the period elongation that took place due to the accumulated damage; as the excitation amplitude increased extra joints opened or slipped which reduced the effective stiffness of the modelled walls. Therefore, the computational model based on DEM considered herein was able to reproduce the propagation of damage along the mortar joints and its effect on period elongation.

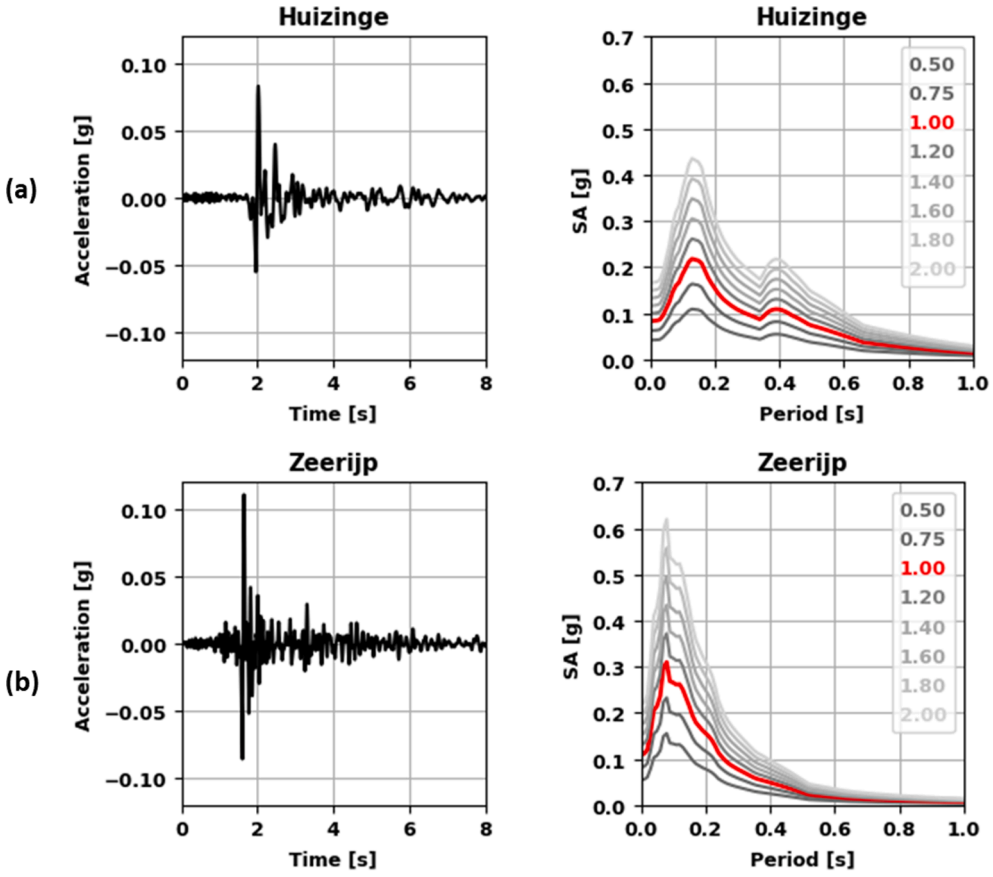

Fig. 10. Acceleration time-history (left) and the corresponding response spectra (right) generated for the IDA are displayed for the (a) Huizinge and (b) Zeerijp records. The legend of graphs with the response spectra (right) denotes the scaling factor used for the IDA.

5. Application of damage indexing to walls under seismic loading

In order to further evaluate the damage propagation on the modelled masonry walls, an incremental dynamic analysis (IDA) was performed [39]. To this end, two records from the Groningen region that produced the highest PGA values were selected [40]. The North component of the MID1 record from the August 2012 Huizinge earthquake (ML 3.6) (Fig. 10a) and the East component of the BGAR record from the January 2018 Zeerijp earthquake (ML 3.4) (Fig. 10b) were used for the analyses. The Huizinge and Zeerijp earthquakes had PGA values 0.08 and 0.11 g respectively [11]. Both records produce spectral acceleration close to 0.15 g for period equal with the natural period of the perforated walls, that is 0.2 s. The records were scaled with factors 0.5, 0.75, 1., 1.2, 1.4, 1.6, 1.8 and 2 and an IDA was performed. During the dynamic analysis, no viscous damping was assumed; instead the only dissipation being due to frictional sliding on the joints.

From the literature review, when no monitoring scheme exists or when testing is unavailable, the inspection process relies on residual signs of damage, that is cracks and drift. In order to provide a better insight of the inflicted damage at the end of the IDAs, the residual *DI* and its components are presented in Fig. 11 for the wall with symmetric opening. The results shown in Fig. 11 correspond to the IDA with the Huizinge record. The residual *DI* was negligible for the lower PGA values and reached 0.11 for the maximum PGA. It is highlighted that the observed residual *DI* was attributed to the components related to cracks, that is DI_{open} and DI_{slip}, while DI_{drift} remained insignificant. Thus, it can be inferred that even though no residual drift was recorded damage could be still observed as cracks. Similar results were also presented by Graziotti et al. [10] where an incremental dynamic shaking table test was performed on a full scale URM house, typical example of the Groningen building stock. In particular, after applying excitations of low amplitude, the residual drift was negligible, but cracks could still be observed on the structure [10].

In Fig. 12 the maximum and residual values of the damage index *DI* as obtained from the IDA results are presented over the maximum attained drift ratios during the analyses. A second order polynomial regression analysis was performed and the produced trendline is shown with blue line in Fig. 12. The data corresponding to the maximum *DI* followed an almost linear increase over the maximum drift ratio as shown from the corresponding trendline (Fig. 12a). The residual *DI* increased linearly before approaching a plateau towards higher drifts.

6. Conclusions

So far, the assessment of damage in masonry structures subjected to dynamic loading is based on post-earthquake observations. However, during earthquake loading, cracks can open and close in a masonry structure. Such opening and closing of cracks is not possible to be identified by post-earthquake observations. The aim of this study was to investigate the quantification of damage on URM structures taking into consideration the initiation and propagation of damage due to recursive earthquake excitations. A dataset of experimental results from in-plane quasi-static cyclic tests on masonry walls was considered. The experimentally obtained crack patterns were investigated and their correlation with damage propagation was studied. Using a software based on the Distinct Element Method (DEM), a numerical model was developed and validated against a series of full-scale experimental tests obtained from the literature. Wall panels representing common typologies of house façades of URM buildings in the Northern European region i.e. Groningen gas field, the Netherlands, were numerically investigated. The accumulated damage within the seismic response of the masonry walls was investigated by means of representative harmonic load excitations and an incremental dynamic analysis based on induced seismicity records from Groningen. A damage index based on cracking formation and drift ratio was proposed and applied to the numerical findings while common trends between the numerical and experimental data were highlighted. Using the results of the developed DEM numerical model, the suitability of the proposed *DI* equation to realistically represent the level of damage and its sensitivity to low amplitude loading was highlighted. The adopted numerical approach was able to capture any residual damage expressed as cracks even when the residual drift was zero at the end of an excitation. Based on the analyses with harmonic loads, the effect of the load amplitude and the period of excitation on the damage propagation was elucidated; when no period resonance took place, the damage was limited even for moderate load amplitude while for the cases that the walls were excited with their natural period, damage was recorded even for lower load amplitudes. Although the proposed approach has been applied to masonry structures subjected to induced seismicity, the methodology could be applied when masonry structures subjected to earthquakes with high aftershock activity.

Additional experimental data with proper documentation of crack propagation are required to provide a generic quantification of damage for different configurations of masonry walls in terms of geometry, boundary conditions, material properties, overload, etc. The proposed damage index *DI* needs to be further calibrated based on experimental findings to correlate the obtained values with damage levels.

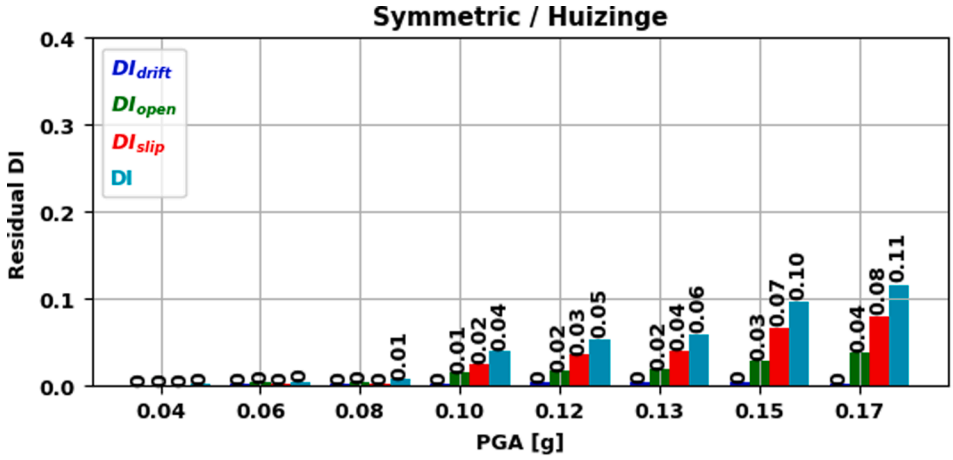

Fig. 11. Residual values of the damage indices DI_{drift}, DI_{open}, DI_{slip} and *DI* presented for the wall with symmetric opening over the corresponding PGA. The results correspond to the IDA with the Huizinge record.

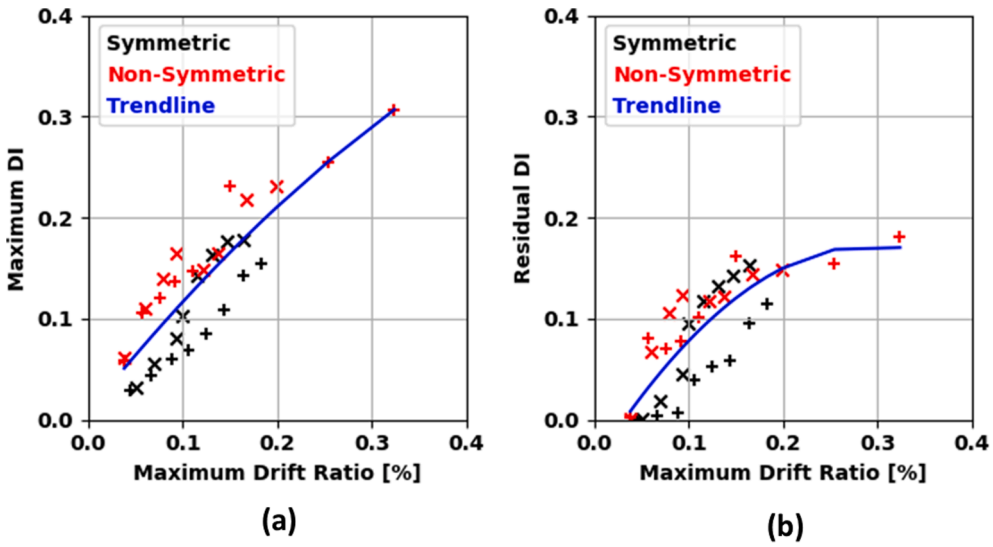

Fig. 12. (a) Maximum and (b) residual values of the damage index **DI** as obtained from the IDA results. The results for the IDA based on the Huizinge and Zeerijp records are shown with '+' and 'x' markers respectively. The trendline obtained from a second order polynomial regression analysis is denoted with blue line. (For interpretation of the references to colour in this figure legend, the reader is referred to the web version of this article.)

CRediT authorship contribution statement

Vasilis Sarhosis: Conceptualization, Methodology, Validation, Visualization, Writing - original draft. **Dimitris Dais:** Conceptualization, Methodology, Data curation, Writing - original draft. **Eleni Smyrou:** Conceptualization, Methodology, Writing - review & editing. **İhsan Engin Bal:** Conceptualization, Methodology, Writing - review & editing. **Anastasios Drougkas:** Visualization, Writing - review & editing.

Declaration of Competing Interest

The authors declare that they have no known competing financial interests or personal relationships that could have appeared to influence the work reported in this paper.

Acknowledgements

The work presented in this paper is supported by the – Seismic Monitoring, Design and Strengthening For thE GrOningen Region, Project number: RAAK.MKB09.021.

References

[1] Foulger GR, Wilson MP, Gluyas JG, Julian BR, Davies RJ. Global review of human-induced earthquakes. Earth-Science Rev 2018;178:438–514. https://doi.org/10.1016/j.earscirev.2017.07.008.
[2] Abbiati G, Broccardo M, Didier M, Beyer K, Stojadinovic B. A probabilistic damage model for predicting plaster cracks on unreinforced masonry walls. 16th Eur. Conf. Earthq. Eng. (ECEE 2018), 2018.
[3] van Thienen-Visser K, Breunese JN. Induced seismicity of the groningen gas field: history and recent developments. Lead Edge 2015;34:664–71. https://doi.org/10.1190/tle34060664.1.
[4] Mulder M, Perey P. Gas Production and Earthquakes in Groningen; Reflection on Economic and Social Consequences. Cent Energy Econ Res (CEER), Policy Pap No 3 Univ Groningen, Netherlands 2018.
[5] Bal İE, Smyrou E, Bulder E. Liability and damage claim issues in induced earthquakes: case of Groningen. SECED 2019 Conf., Greenwich, UK: 2019.
[6] Crowley H, Pinho R, Polidoro B, van Elk J. Developing fragility and consequence models for buildings in the Groningen field. Netherlands J Geosci 2017;96:s247–57. https://doi.org/10.1017/njg.2017.36.
[7] Godio M, Vanin F, Zhang S, Beyer K. Quasi-static shear-compression tests on stone masonry walls with plaster: Influence of load history and axial load ratio. Eng Struct 2019;192:264–78. https://doi.org/10.1016/j.engstruct.2019.04.041.
[8] Beyer K, Mergos P. Sensitivity of drift capacities of URM Walls to cumulative damage demands and implication on loading protocols for quasi-static cyclic tests. 12th North Am. Mason. Conf., Denver, Colorado, USA: 2015.
[9] Korswagen PA, Longo M, Meulman E, Rots JG. Crack initiation and propagation in unreinforced masonry specimens subjected to repeated in-plane loading during light damage. Bull Earthq Eng 2019;17:4651–87. https://doi.org/10.1007/s10518-018-00553-5.
[10] Graziotti F, Tomassetti U, Kallioras S, Penna A, Magenes G. Shaking table test on a full scale URM cavity wall building. Bull Earthq Eng 2017;15:5329–64. https://doi.org/10.1007/s10518-017-0185-8.
[11] Sarhosis V, Dais D, Smyrou E, Bal İE. Evaluation of modelling strategies for estimating cumulative damage on Groningen masonry buildings due to recursive induced earthquakes. Bull Earthq Eng 2019;17:4689–710. https://doi.org/10.1007/s10518-018-00549-1.
[12] Gonçalves LM da S, Rodrigues H, Gaspar F. Nondestructive Techniques for the Assessment and Preservation of Historic Structures. Boca Raton: CRC Press; 2017. https://doi.org/10.1201/9781315168685.
[13] Saisi A, Gentile C. Post-earthquake diagnostic investigation of a historic masonry tower. J Cult Herit 2015;16:602–9. https://doi.org/10.1016/j.culher.2014.09.002.
[14] Erdik M. Seismic Isolation, Structural Health Monitoring, and Performance Based Seismic Design in Earthquake Engineering. Cham: Springer International Publishing; 2019. https://doi.org/10.1007/978-3-319-93157-9.
[15] Bal İE, Dais D, Smyrou E, Sarhosis V. Monitoring of a historical masonry structure in case of induced seismicity. Int J Archit Herit 2020. https://doi.org/10.1080/15583058.2020.1719230.
[16] Salmanpour A, Mojsilović N, Schwartz J. Displacement capacity of contemporary unreinforced masonry walls: an experimental study. Eng Struct 2015;89:1–16. https://doi.org/10.1016/j.engstruct.2015.01.052.
[17] Shafiei Dizaji M, Alipour M, Harris DK. Leveraging Full-Field Measurement from 3D Digital Image Correlation for Structural Identification. Exp Mech 2018;58:1049–66. https://doi.org/10.1007/s11340-018-0401-8.
[18] Acikgoz S, DeJong MJ, Soga K. Sensing dynamic displacements in masonry rail bridges using 2D digital image correlation. Struct Control Heal Monit 2018;25:1–24. https://doi.org/10.1002/stc.2187.
[19] Vanniamparambil PA, Bolhassani M, Carmi R, Khan F, Bartoli I, Moon FL, et al. A data fusion approach for progressive damage quantification in reinforced concrete masonry walls. Smart Mater Struct 2014;23:015007. https://doi.org/10.1088/0964-1726/23/1/015007.
[20] Shetty N, Livitsanos G, Van Roy N, Aggelis DG, Van Hemelrijck D, Wevers M, et al. Quantification of progressive structural integrity loss in masonry with acoustic emission-based damage classification. Constr Build Mater 2019;194:192–204. https://doi.org/10.1016/j.conbuildmat.2018.10.215.
[21] Carrillo J, Dominguez D, Prado N. Seismic damage index based on fractal dimension of cracking on thin reinforced concrete walls. ACI Struct J 2017;114. https://doi.org/10.14359/51700919.
[22] Farhidzadeh A, Dehghan-Niri E, Moustafa A, Salamone S, Whittaker A. Damage Assessment of Reinforced Concrete Structures Using Fractal Analysis of Residual Crack Patterns. Exp Mech 2013;53:1607–19. https://doi.org/10.1007/s11340-013-9769-7.
[23] FEMA 307. Evaluation of Earthquake Damaged Concrete and Masonry Wall Buildings: Technical Resources. The Applied Technology Council; 1998.
[24] Zaborac J, Athanasiou A, Salamone S, Bayrak O, Hrynyk TD. Crack-based shear strength assessment of reinforced concrete members using a fixed-crack continuum modeling approach. J Struct Eng 2020;146:04020024. https://doi.org/10.1061/(ASCE)ST.1943-541X.0002564.

[25] Carrillo J, Alcocer SM. Acceptance limits for performance-based seismic design of RC walls for low-rise housing. Earthq Eng Struct Dyn 2012;41:2273–88. https://doi.org/10.1002/eqe.2186.
[26] Lattanzi D, Miller GR, Eberhard MO, Haraldsson OS. Bridge column maximum drift estimation via computer vision. J Comput Civ Eng 2015;30. https://doi.org/10.1061/(ASCE)CP.1943-5487.0000527.
[27] Davoudi R, Miller GR, Kutz JN. Data-driven vision-based inspection for reinforced concrete beams and slabs: Quantitative damage and load estimation. Autom Constr 2018;96:292–309. https://doi.org/10.1016/j.autcon.2018.09.024.
[28] Giamundo V, Sarhosis V, Lignola GP, Sheng Y, Manfredi G. Evaluation of different computational modelling strategies for the analysis of low strength masonry structures. Eng Struct 2014;73:160–9. https://doi.org/10.1016/j.engstruct.2014.05.007.
[29] FEMA. FEMA-356: Prestandard and Commentary for the Seismic Rehabilitation of Buildings. Washington, D.C.: FEMA; 2000.
[30] ASCE. ASCE/SEI 7-16: Minimum Design Loads and Associated Criteria for Buildings and Other Structures. ASCE/SEI 7. American Society of Civil Engineers; 2017. https://doi.org/10.1061/9780784414248.
[31] EN-1998-1. Eurocode 8, Design of Structures for Earthquake Resistance, Part 1: General rules, seismic actions and rules for buildings. Brussels: European Committee for Standardization; 2005.
[32] NTC. Decreto Ministeriale 14/1/2008. Norme tecniche per le costruzioni, Ministry of infrastructures and transportations. G.U. S.O. n.30 on 4/2/2008 (in Italian). 2008.
[33] Burland JB, Wroth CP. Settlement of buildings and associated damage. Settl. Struct. Proc. Conf. Br. Geotech. Soc. 1974:611–54.
[34] Cundall PA. A computer model for simulating progressive large scale movements in blocky rock systems. Proc. Symp. Int. Soc. Rock Mech, Nancy, 1971.
[35] ITASCA. UDEC—universal distinct element code manual: theory and background. Itasca Consulting Group, Minneapolis 2011.
[36] Sarhosis V, Sheng Y. Identification of material parameters for low bond strength masonry. Eng Struct 2015;60:100–10.
[37] Lemos JV. Discrete element modeling of masonry structures. Int J Archit Herit 2007;1:190–213. https://doi.org/10.1080/15583050601176868.
[38] Cundall PA, Hart RD. Numerical Modeling of Discontinua. Anal. Des. Methods, Elsevier 1993:231–43. https://doi.org/10.1016/B978-0-08-040615-2.50015-0.
[39] Vamvatsikos D, Cornell CA. Incremental dynamic analysis. Earthq Eng Struct Dyn 2002;31:491–514. https://doi.org/10.1002/eqe.141.
[40] Bal İE, Smyrou E, Dais D. Comparison of polarity in Groningen data with that of other natural and induced seismicity records, and implications in hazard and risk models. Bull Earthq Eng 2019;17:4457–74. https://doi.org/10.1007/s10518-018-0517-3.
[41] Sarhosis V, Lemos JV. Detailed micro-modelling of masonry using the discrete element method. Comput Struct 2018;206:66–81. https://doi.org/10.1016/j.compstruc.2018.06.003.
[42] Downey A, D'Alessandro A, Laflamme S, Ubertini F. Smart bricks for strain sensing and crack detection in masonry structures. Smart Mater. Struct. 2018;27:015009. https://doi.org/10.1088/1361-665X/aa98c2.
[43] Ferrante A, Clementi F, Milani G. Advanced numerical analyses by the non-smooth contact dynamics method of an ancient masonry bell tower. ICNAAM 2019;43(13):7706–25. https://doi.org/10.1002/mma.6113.
[44] Milani G, Lourenço PB, Tralli A. Homogenised limit analysis of masonry walls, Part I: failure surfaces. Comput Struct 2006;84(3–4):166–80. https://doi.org/10.1016/j.compstruc.2005.09.005.